LUND UNIVERSITY

Estimating radar positions using unmanned air vehicle teams engaged in cooperative deception

Purvis, K.B.; Åström, Karl Johan; Khammash, M. H.

[Link to publication](#)

Estimating Radar Positions Using Cooperative Unmanned Air Vehicle Teams

Keith B. Purvis
kpurvis@engineering.ucsb.edu

Karl J. Åström
astrom@engineering.ucsb.edu

Mustafa Khammash
khammash@engineering.ucsb.edu

Abstract— Standard TDOA (Time-Difference of Arrival) estimation techniques are modified and applied to locate networked enemy radars using a cooperative team of unmanned Electronic Combat Air Vehicles (ECAVs). The team is engaged in deceiving the radars, which limits where the ECAVs can fly and requires accurate radar positions to be known. Two TDOA measurements of radar pulses taken by two ECAV pairs are used to estimate the position of the middle radar. A nonlinear system model for estimation is formulated and used to perform simulations with "noisy" TDOAs; a linearized time-varying model for straight nominal ECAV trajectories is derived from the nonlinear model. The choice of optimal ECAV trajectories and an observer to minimize the variance of the middle radar position—using the linearized model—is addressed. Application of a time-varying Kalman Filter to the linearized system shows drastic improvement in reducing the variance of position estimates when compared to the original nonlinear system via simulations.

I. INTRODUCTION

The Estimation Problem here is connected to the Cooperative Deception Problem in [1], [2]: using unmanned Electronic Combat Air Vehicles (ECAVs) to cooperatively deceive an enemy radar network by causing the network to detect and track the motion of a phantom or nonexistent air vehicle. A radar network is defined as two or more radars that share track files to correlate a target. Methods for generating a phantom target are restricted to range-delay techniques applied through the radar mainlobe. For a team of ECAVs—generally one per radar—to succeed against the radar network, each ECAV's trajectory must satisfy several dynamic limitations in [2]; also, each radar's position must be accurately known by the ECAV assigned to it.

Radar position estimation is addressed using TDOA (Time-Difference of Arrival) techniques. To generate a TDOA measurement, each of two ECAVs uses a synchronized internal clock to record a time stamp on the arrival of a unique encoded radar pulse, and the difference between the two times is taken. Knowledge of one TDOA places the transmitting radar on a hyperbolic curve on the ground. Thus, based on two or more measurements, the radar's position can be estimated by taking the (correct) intersection of the hyperbolas. The estimate will not be exact due to electronic measurement noise and synchronization error of

the ECAV clocks, which is based on using GPS for timing; see [3] and chapter 11 of [4] for more details.

One key point is that the choice of ECAV trajectories flown significantly affects the accuracy of the radar position estimates determined through TDOA techniques. Hence, it is important to find ECAV trajectories that will minimize the variance of these estimates. Another key point is that even the best ECAV trajectories will cause unacceptable variance in the radar position estimates; however, knowing the distribution of the TDOA measurement error allows effective filtering of the estimation system. Assuming a Gaussian distribution, a time-varying Kalman Filter applied to a linearized position estimation system can significantly reduce the variance of estimates as compared to the original unfiltered nonlinear system. Again, minimizing this variance through filtering and selection of optimal ECAV control inputs/trajectories will then maximize the coherency of the phantom track for the radar network.

II. THE DECEPTION PROBLEM BACKGROUND

Assuming that an ECAV is stealthy and knows the maximum operational range, R_{max}, and location of a radar with pulse-to-pulse agility, the ECAV can intercept and send delayed returns of the radar's transmitted pulses so that the radar sees a phantom target at a range beyond the ECAV but closer than R_{max}. Fig. 1 illustrates how three ECAVs could cooperatively create a single phantom track by using range-delay; this figure defines the constant-elevation scenario that will be used for the Estimation Problem from here on.

To move with the phantom track in Fig. 1, each ECAV behaves much like a bead on a string that is rotating at some variable rate; the ECAV may slide up or down freely but must rotate with the LOS (line of sight) from the radar to the phantom track. An ECAV trying to generate a given phantom track will have one constraint, θ, and one DOF (degree of freedom). To fully define an ECAV trajectory, this remaining DOF is then constrained by specifying any other ECAV variable of motion. Fig. 2 relates the relevant variables, where E is ECAV and T is phantom target.

Without loss of generality, $\dot{\theta}$ is assumed positive and given by the pre-determined phantom track. Parametric equations for the track in Fig. 1 are given below; see Fig. 2 for most of the variables used. The phantom track angle (between each radar's initial LOS and the track heading), ψ_i, and initial range, R_{0i}, are different for each radar, where
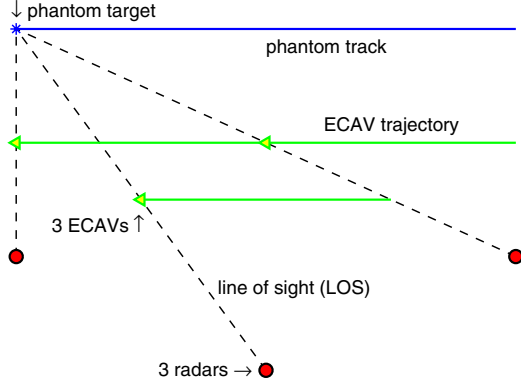
Fig. 1. Cooperative Deception of a Three-Radar Network by ECAVs Generating a Straight Phantom Track

Fig. 2. ECAV and Phantom Track Variables and Their Relations

i indexes the radar/ECAV pairs from left to right in Fig. 1.

$$R_i(t) = \sqrt{R_{0i}^2 + \upsilon_T^2 t^2 - 2R_{0i}\upsilon_T t \cos \psi_i} \qquad (1)$$

$$\theta_i(t) = \arcsin \left(\frac{\upsilon_T t \sin \psi_i}{R_i(t)} \right) \qquad (2)$$

$$\dot{\theta}_i(t) = \frac{R_{0i}\upsilon_T \sin \psi_i}{R_i^2(t)} \qquad (3)$$

To create the phantom track, each ECAV flies a bearing from its radar of $\theta_i(t)$ and uses range-delay techniques to create a phantom target at the range $R_i(t)$. Since a reasonable way to control an ECAV is to steer it by way of a rudder, a dynamical system is sought that describes the motion of the ECAV in terms of its course, ϕ_{Ei}, as the input (for simplicity, the dynamics between the rudder fin and ECAV course are neglected). The following nonautonomous system, derived from Fig. 2, is used for this purpose.

$$\dot{r}_i(t) = r_i \dot{\theta}_i(t) \cot \phi_{Ei}, \quad r_i(0) = r_{0i} \qquad (4)$$

Based on the ECAV dynamics, ϕ_{Ei} is restricted to be piecewise continuously differentiable. Since $\dot{\theta}_i$ cannot be zero, $0 < \phi_{Ei} < \pi$ is also required. Once the ith ECAV has chosen its course $\phi_{Ei}(t)$, its range $r_i(t)$ is completely specified by (4); this profile, together with $\theta_i(t)$ from the given phantom track, completely defines the ECAV's trajectory, which may be solved using (1)–(4). Note that, to remain in sync with the phantom track, the ECAV must constantly adjust its speed to satisfy $\upsilon_E = \sqrt{(r\dot{\theta})^2 + (\dot{r})^2}$.

III. Details of TDOA Position Estimation

In measuring TDOAs, it is assumed that the ECAVs have GPS-synchronized clocks and that each ECAV is able to detect pulses projected from radar sidelobes, which are much weaker in power than pulses from the mainlobe. To simplify analysis, only the position of the middle radar is estimated using two TDOA measurements[1] from ECAV

[1]If more than two measurements are used, then the system of equations is overdetermined, and methods such as nonlinear least squares may be used as in [5] to find the "average" position estimate.
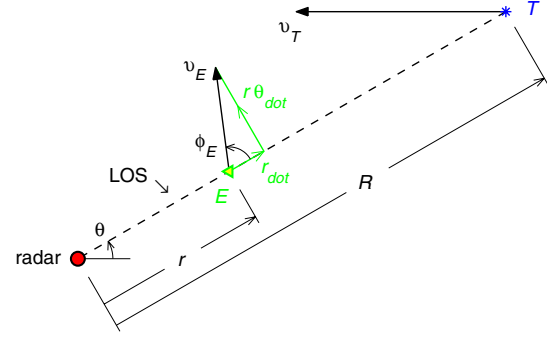

Fig. 3. Estimation of Middle Radar Position by Three ECAVs Using TDOA Techniques, without Noise

pairs 1-2 and 3-2. With only two hyperbolas generated by these measurements, more than one intersection will result as in Fig. 3; however, the correct intersection nearest the true position of the middle radar can be uniquely identified by discriminating all intersections as the ECAVs move or assuming a general location for the radar is already known. Finally, the variance of the middle radar's position estimate is not injected back into the phantom track equations used by the middle ECAV to fly its trajectory.

Fig. 3 illustrates how two noise-free TDOA measurements are used to determine the position of the middle radar. The two hyperbolas in the figure correspond to the TDOAs converted to distance-differences in the following two equations. In these equations, c is the speed of light and τ_i is the arrival time of the middle radar pulse at the ith ECAV; the other variables used are shown in Fig. 3.

$$\Delta_1 := c \overbrace{(\tau_1 - \tau_2)}^{\text{TDOAs}} = d_1 - r_2 \qquad (5)$$

$$\Delta_3 := c (\tau_3 - \tau_2) = d_3 - r_2 \qquad (6)$$

Only Δ_1 and Δ_3 can be measured—the arrival times and distances are unknown. With white noise injected into the TDOA measurements to approximate the combined effect

(a) Parallel with Phantom Track   (b) Circular around Radars

Fig. 4. Variance of Radar Position Estimates over Time for Different ECAV Trajectories but Identical Distributions of Measurement Noise
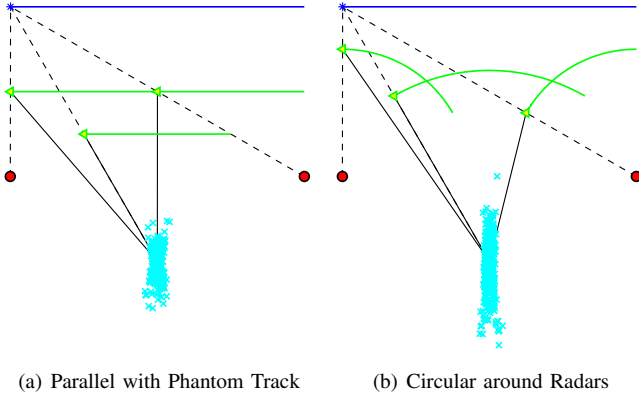
of electronic measurement noise and synchronization error of the ECAV clocks[2], hyperbolic bands are created due to the variation in TDOA measurements over time while the ECAVs remain fixed in place. Intuitively, the variance of the radar position estimates due to noise will be minimized when the ECAVs are more spread apart in angle.

Fig. 4(a) shows typical position estimates of the middle radar calculated over time as the ECAVs fly from right to left, parallel to the phantom track. Fig. 4(b) differs only in the circular ECAV trajectories about each radar. In the first scenario, the position estimates are scattered significantly in range as well as in angle; in the second, the position estimates are scattered more in range and less in angle. Thus, Fig. 4 shows that different ECAV trajectories can significantly change the variance of radar position estimates when TDOA techniques are used, which motivates the need for a minimum-variance control strategy for the ECAVs. In addition, it was verified that even the better ECAV trajectories produce unacceptable error in position estimates when TDOA estimation is used without filtering.

IV. NONLINEAR AND LINEAR ESTIMATION MODELS

To minimize the variance of the radar position estimates—in this case, only the position estimates of the middle radar—a nonlinear TDOA estimation model is presented and then linearized about reasonable nominal ECAV trajectories. Let (x_0, y_0) be the true position of the middle radar and e_i a Wiener process, then introduce the following.

$$\boldsymbol{\xi} := \begin{bmatrix} r_1 & r_2 & r_3 & x_0 & y_0 \end{bmatrix}^{\mathrm{T}}$$
$$\boldsymbol{u} := \begin{bmatrix} \phi_{E1} & \phi_{E2} & \phi_{E3} \end{bmatrix}^{\mathrm{T}}$$
$$\boldsymbol{\eta} := \begin{bmatrix} \Delta_1 & \Delta_3 \end{bmatrix}^{\mathrm{T}}$$
$$\frac{\mathrm{d}\boldsymbol{e}}{\mathrm{d}t} := \begin{bmatrix} \frac{\mathrm{d}e_1}{\mathrm{d}t} & \frac{\mathrm{d}e_3}{\mathrm{d}t} \end{bmatrix}^{\mathrm{T}}$$

The state, $\boldsymbol{\xi}$, contains the ranges for each ECAV from its respective radar, and the actual position of the middle radar.

---

[2]A first-order Guass-Markov process would be more accurate here according to [4], but a Gaussian random process is used for simplicity.

The control input, $\boldsymbol{u}$, contains the courses for each ECAV relative to its bearing θ_i (see Fig. 2 above). The measured output, $\boldsymbol{\eta}$, contains the actual TDOA measurements converted to distance as shown in (5)–(6), and the white noise, $\frac{\mathrm{d}\boldsymbol{e}}{\mathrm{d}t}$, represents TDOA measurement error.

The nonlinear system for TDOA estimation of the middle radar position formally becomes the following, by using (1)–(6); (x_i, y_i) is the position of the ith ECAV, and (p_{xi}, p_{yi}) is the position of the ith radar.

$$\dot{\boldsymbol{\xi}} = \begin{bmatrix} r_1\dot{\theta}_1(t)\cot\phi_{E1} \\ r_2\dot{\theta}_2(t)\cot\phi_{E2} \\ r_3\dot{\theta}_3(t)\cot\phi_{E3} \\ 0 \\ 0 \end{bmatrix} = \boldsymbol{f}(\boldsymbol{\xi}, \boldsymbol{u}, t) \tag{7}$$

$$\boldsymbol{\eta} = \begin{bmatrix} \sqrt{(x_1(t) - x_0)^2 + (y_1(t) - y_0)^2} - r_2 \\ \sqrt{(x_3(t) - x_0)^2 + (y_3(t) - y_0)^2} - r_2 \end{bmatrix} + \frac{\mathrm{d}\boldsymbol{e}}{\mathrm{d}t}$$
$$= \boldsymbol{g}(\boldsymbol{\xi}, t) + \frac{\mathrm{d}\boldsymbol{e}}{\mathrm{d}t}, \tag{8}$$

where

$$x_i(t) = p_{xi} + r_i\cos(\theta_i(t) + \psi_i)$$
$$y_i(t) = p_{yi} + r_i\sin(\theta_i(t) + \psi_i)$$

Linearizing around a trajectory $(\boldsymbol{\xi}(t), \boldsymbol{u}(t))_{nom}$ gives

$$\dot{\boldsymbol{\delta\xi}} = A(t)\boldsymbol{\delta\xi} + B(t)\boldsymbol{\delta u}$$
$$\boldsymbol{\delta\eta} = C(t)\boldsymbol{\delta\xi} + 0\,\boldsymbol{\delta u} + \frac{\mathrm{d}\boldsymbol{e}}{\mathrm{d}t},$$

where the Jacobians $\frac{\partial \boldsymbol{f}}{\partial \boldsymbol{\xi}}$, $\frac{\partial \boldsymbol{f}}{\partial \boldsymbol{u}}$, and $\frac{\partial \boldsymbol{g}}{\partial \boldsymbol{\xi}}$ are evaluated at the nominal trajectory to get $A(t)$, $B(t)$, and $C(t)$, respectively.

The nominal control input and corresponding trajectory for the system state are chosen so that each ECAV flies parallel to the phantom track as in Fig. 1, hence

$$\boldsymbol{u}_{nom}(t) = \begin{bmatrix} \pi - \psi_1 - \theta_1(t) \\ \pi - \psi_2 - \theta_2(t) \\ \pi - \psi_3 - \theta_3(t) \end{bmatrix} = \begin{bmatrix} 5\pi/6 - \theta_1(t) \\ 2\pi/3 - \theta_2(t) \\ \pi/2 - \theta_3(t) \end{bmatrix} \text{ rad}$$
$$\boldsymbol{\xi}_{nom}(t) = \begin{bmatrix} R_1(t)/2 & R_2(t)/2 & R_3(t)/2 & 0 & 0 \end{bmatrix}^{\mathrm{T}} \text{ km.}$$

In reality, the last two components of $\boldsymbol{\xi}_{nom}$ would be an initial guess for (x_0, y_0); however, the true position is used here to show the theoretical best-case performance for estimation. The linearized equations can be written as

$$\dot{\boldsymbol{\delta\xi}}_i = \begin{cases} \dot{\theta}_i \cot \boldsymbol{u}_{nom_i}\boldsymbol{\delta\xi}_i - \frac{R_i\dot{\theta}_i}{2\sin^2\boldsymbol{u}_{nom_i}}\boldsymbol{\delta u}_i & i = 1,2,3 \\ 0 & i = 4,5 \end{cases} \tag{9}$$

$$\boldsymbol{\delta\eta} = \begin{bmatrix} c_{11} & c_{12} & c_{13} & c_{14} & c_{15} \\ c_{21} & c_{22} & c_{23} & c_{24} & c_{25} \end{bmatrix} \boldsymbol{\delta\xi} + \frac{\mathrm{d}\boldsymbol{e}}{\mathrm{d}t}, \tag{10}$$

where

$$c_{11} = \frac{x_1{}^{nom}\cos(\theta_1 + \pi/6) + y_1{}^{nom}\sin(\theta_1 + \pi/6)}{d_1{}^{nom}}$$

$$c_{12} = c_{22} = -1$$

$$c_{13} = c_{21} = 0$$

$$c_{14} = -x_1{}^{nom}/d_1{}^{nom}$$

$$c_{15} = -y_1{}^{nom}/d_1{}^{nom}$$

$$c_{23} = \frac{x_3{}^{nom}\cos(\theta_3 + \pi/2) + y_3{}^{nom}\sin(\theta_3 + \pi/2)}{d_3{}^{nom}}$$

$$c_{24} = -x_3{}^{nom}/d_3{}^{nom}$$

$$c_{25} = -y_3{}^{nom}/d_3{}^{nom},$$

and R_i, θ_i, $\dot{\theta}_i$, $\boldsymbol{u}_{nom_i}$, x_i, y_i, and d_i (see Fig. 3 above) are functions of time. The superscript nom indicates that nominal values have been substituted in for state variables. The parameters for (p_{xi}, p_{yi}), ψ_i, and R_{0i} were chosen to match Fig. 1, where the phantom track length is 26 km.

The linearized system (9)–(10) was confirmed observable except at the initial and final times (observability does not hold in general for all $\boldsymbol{\xi}_{nom}, \boldsymbol{u}_{nom}$—take e.g. the Fig. 4(b) scenario). The average condition number of the observability matrix was approximately 1000. Thus, the middle radar position may be observed through the measured output, and the estimate will be sensitive to measurement error.

V. Minimum Variance Estimation Theory

Given a general linear system model in the form of a stochastic differential equation (see [6] for theory),

$$\mathrm{d}\boldsymbol{\xi} = A(t)\boldsymbol{\xi}\,\mathrm{d}t + B(t)\boldsymbol{u}\,\mathrm{d}t + \mathrm{d}\boldsymbol{v} \tag{11}$$

$$\boldsymbol{\eta}\,\mathrm{d}t = C(t)\boldsymbol{\xi}\,\mathrm{d}t + \mathrm{d}e, \tag{12}$$

where $\boldsymbol{v}$ and e are independent Wiener processes with zero mean and incremental covariances of $R_{\boldsymbol{v}}\mathrm{d}t$ and $R_{\boldsymbol{e}}\mathrm{d}t$, the minimum variance observer and observer error are

$$\mathrm{d}\hat{\boldsymbol{\xi}} = A(t)\hat{\boldsymbol{\xi}}\,\mathrm{d}t + B(t)\boldsymbol{u}\,\mathrm{d}t + K(t)\left[\boldsymbol{\eta}\,\mathrm{d}t - C(t)\hat{\boldsymbol{\xi}}\,\mathrm{d}t\right] \tag{13}$$

$$\mathrm{d}\tilde{\boldsymbol{\xi}} = [A(t) - K(t)C(t)]\,\tilde{\boldsymbol{\xi}}\,\mathrm{d}t + \mathrm{d}\boldsymbol{v} + K(t)\mathrm{d}e, \tag{14}$$

$$K(t) = P(t)C^{\mathrm{T}}(t)R_{\boldsymbol{e}}{}^{-1}, \tag{15}$$

$$\frac{\mathrm{d}P}{\mathrm{d}t} = A(t)P + PA^{\mathrm{T}}(t) + R_{\boldsymbol{v}} - PC^{\mathrm{T}}(t)R_{\boldsymbol{e}}{}^{-1}C(t)P,$$
$$P(0) = P_0. \tag{16}$$

Above, $K(t)$ is the observer gain, $\hat{\boldsymbol{\xi}}$ is the estimate of the state, and $\tilde{\boldsymbol{\xi}} := \boldsymbol{\xi} - \hat{\boldsymbol{\xi}}$ is the error. The state covariance matrix is $P(t) := \mathrm{E}(\tilde{\boldsymbol{\xi}}\tilde{\boldsymbol{\xi}}^{\mathrm{T}})$, where E is the expectation. $R_{\boldsymbol{v}} = 0$ because there is assumed no noise in the ECAV dynamics, and P_0 must be chosen.

VI. The Linearized System with Observer

Because the linearized system (9)–(10) fits the form in (11)–(12) and is observable, it is a suitable candidate for applying the time-varying Kalman Filter or observer in (13) and (15)–(16) to estimate the position of the middle radar. The block diagram in Fig. 5 shows the basic scheme for this
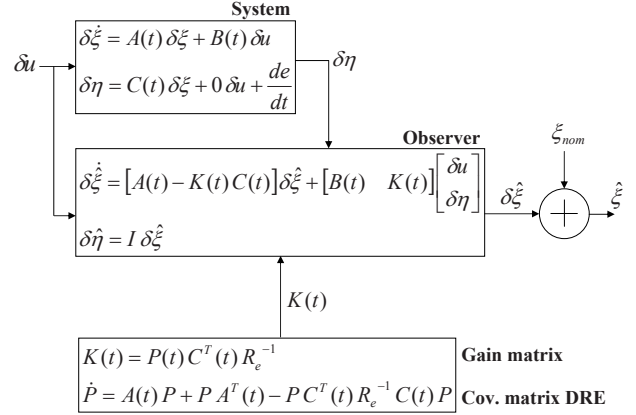

Fig. 5. Block Diagram of the Linearized Filtered System for Estimation

design. The overall system contains 25 state variables: 5 for $\boldsymbol{\delta\xi}$, 5 for $\boldsymbol{\delta\hat{\xi}}$, and 15 for P, which is symmetric. Simulations following use the scheme in Fig. 5 to assess the observer's theoretical best-case performance with $\boldsymbol{\xi}_{nom}$ known. For practical implementation, the true nominal position of the middle radar will be unknown; thus, an estimate must be used for $\boldsymbol{\xi}_{nom}$, which will add a bias to $\hat{\boldsymbol{\xi}}$ and change the linearized matrices in the observer. The matrices of the linearized system itself will not be affected because they model physical reality, i.e. what is actually measured based on the true position of the radar. Preliminary experiments indicate that bringing the full measurement $\boldsymbol{\eta}$ into the observer and updating online the estimate for $\boldsymbol{\xi}_{nom}$ is a workable solution to this problem.

Since only the last two system state variables are estimated, and those two state variables have no dynamics, most of the components of P and terms in (16) are zero. The differential equation for the *nonzero* terms of P—a subset of the last term for $\frac{\mathrm{d}P}{\mathrm{d}t}$ in (16)—is shown below, where p_{44} and p_{55} are the variance of the middle radar position estimates, $\hat{x}_0$ and $\hat{y}_0$, respectively. The scalar R_e represents the noise intensity for each of the TDOA measurements. Recall that (x_i, y_i) and d_i are the ECAV positions and distances to the middle radar, and the superscript nom means that nominal values have replaced state variables.

$$\begin{bmatrix} \dot{p}_{44} & \dot{p}_{45} \\ \dot{p}_{45} & \dot{p}_{55} \end{bmatrix} =: \dot{\bar{P}} = -\frac{1}{R_e}\bar{P}\bar{C}^{\mathrm{T}}(t)\bar{C}(t)\bar{P}, \tag{17}$$

$$\bar{C}(t) = \begin{bmatrix} -x_1{}^{nom}/d_1{}^{nom} & -y_1{}^{nom}/d_1{}^{nom} \\ -x_3{}^{nom}/d_3{}^{nom} & -y_3{}^{nom}/d_3{}^{nom} \end{bmatrix}$$

Rewriting (17) in component-form and using the fact that the middle radar is located at the origin gives

$$\dot{p}_{44} = \frac{-1}{R_e}\left[\frac{\left(\frac{x_1{}^{nom}}{y_1{}^{nom}}p_{44} + p_{55}\right)^2}{\left(\frac{x_1{}^{nom}}{y_1{}^{nom}}\right)^2 + 1} + \frac{\left(\frac{x_3{}^{nom}}{y_3{}^{nom}}p_{44} + p_{45}\right)^2}{\left(\frac{x_3{}^{nom}}{y_3{}^{nom}}\right)^2 + 1}\right] \tag{18}$$

$$\dot{p}_{55} = \frac{-1}{R_e}\left[\frac{\left(\frac{y_1{}^{nom}}{x_1{}^{nom}}p_{55} + p_{45}\right)^2}{\left(\frac{y_1{}^{nom}}{x_1{}^{nom}}\right)^2 + 1} + \frac{\left(\frac{y_3{}^{nom}}{x_3{}^{nom}}p_{55} + p_{45}\right)^2}{\left(\frac{y_3{}^{nom}}{x_3{}^{nom}}\right)^2 + 1}\right]. \tag{19}$$

Using (17)–(19), the following theorem is now proven.

Theorem 1: Consider the linearized equations (9)–(16), which are connected as shown in Fig. 5. If the middle radar is stationary, then the variance of its position estimates, $p_{44} + p_{55}$, converges to zero.

Proof: Based on the physical constraints of the Cooperative Deception Problem, ECAVs 1 and 3 will never fly opposed at 0 or 180 degrees relative to the middle radar; continuing with this fact, get

$$\Leftrightarrow \quad \frac{x_1}{y_1} \neq \frac{x_3}{y_3} \Leftrightarrow x_1 y_3 - x_3 y_1 \neq 0$$

$$\Leftrightarrow \quad \det \bar{C} = \frac{(x_1 y_3)^{nom} - (x_3 y_1)^{nom}}{(d_1 d_3)^{nom}} \neq 0.$$

Setting $\dot{\bar{P}}$ to zero in (17) and with $\bar{C}$ now invertible, get

$$0 = \bar{P} \bar{C}^{\mathrm{T}} \bar{C} \bar{P} = \left(\bar{C} \bar{P} \right)^{\mathrm{T}} \left(\bar{C} \bar{P} \right)$$

$$\Leftrightarrow \bar{C} \bar{P} = 0 \Leftrightarrow \bar{P} = 0,$$

which shows that 0 is the unique equilibrium for $\bar{P}$. Finally, (18) and (19) show that $\dot{p}_{44}$ and $\dot{p}_{55}$ are nonpositive, which means that p_{44} and p_{55} are monotonically nonincreasing. Also, by definition p_{44} and p_{55} are bounded below by zero. Therefore, $\lim p_{44}$ and $\lim p_{55}$ exist and must equal 0. ∎

Steady-state will not be reached in practice since the deception process occurs in a short time. It is therefore desirable that the variance of the position estimates decrease as rapidly as possible over this time interval. Observing (17), the rate of change of $\bar{P}$ can be altered by choosing a *different nominal trajectory* for linearizing (7)–(8). Choosing $\boldsymbol{u}_{nom}(t)$ determines $\boldsymbol{\xi}_{nom}(t)$, which completely specifies $\bar{C}(t)$ in (17) through the nominal ECAV positions, $(x_i{}^{nom}(t), y_i{}^{nom}(t))$, and their distances to the middle radar, $d_i{}^{nom}(t)$. Thus, $\boldsymbol{u}_{nom}(t)$ should be chosen to make $\dot{p}_{44}$ and $\dot{p}_{55}$ in (17) or (18)–(19) as negative as possible. This insight shows how selecting an optimal nominal control input could help to further decrease the variance of the middle radar position estimates over a finite time interval.

VII. Simulations of the Nonlinear System and Linearized System with Observer

The linearized system with observer in Fig. 5 is now compared with the nonlinear system (7)–(8) for position estimation of the middle radar. The equations are integrated in MATLAB using "`ode45`" with results shown in Fig. 6. Deviations from the nominal control input are chosen to shift the nominal heading of the ECAVs by ± 7.5 degrees. The phantom track has a speed of 200 m/s, and the ECAVs fly within 20% of 100 m/s. The deception process requires approximately 130 seconds. The noise intensity of each TDOA measurement is set to $R_e = 0.0001$ km^2/Hz, which corresponds to a measurement/synchronization error of 30 m (1σ) with a measurement taken every 0.1 seconds. For the linearized system, an arbitrary choice is made for the initial position estimate. For each simulation, an aerial view of the scenario is shown at the top with the middle radar position estimates of the nonlinear and linear systems magnified by factors of 3 and 50, respectively, for observation. The time average of the variance of the estimates is plotted at the bottom for the nonlinear system. For the linear system, the time average and the ensemble average, $p_{44} + p_{55}$, are both plotted at the bottom.

In Fig. 6(a) where the ECAVs fly toward the radars, the variance of the position estimates approaches 0.1 km^2 at the end of the time interval. In contrast, Fig. 6(b) where the ECAVs move away from the radars shows this variance increasing to approximately 0.3 km^2. The key difference between these two scenarios is that, as time increases, the ECAVs are more spread apart in angle relative to the middle radar when they fly *toward* the radars. Even though certain ECAV trajectories do result in lower variance, it is too large for successful deception.

For the same ECAV trajectories, Fig. 6(c) and Fig. 6(d) show the performance of the filtered linearized system. The estimation accuracy is much improved. The variance of the position estimates reaches 2×10^{-5} km^2 (standard deviation of 4 m) at the end of the deception process with an initial position estimate error for the middle radar of 0.05 km and 0.1 km in the x and y directions, respectively. As shown earlier in Theorem 1, the variance of these estimates converges to zero, but only as time goes to infinity. The difference in the time and ensemble averages of the variance for the linearized system diminishes as time increases. A nice feature of the linearized filtered system is that the initial conditions of the covariance matrix can be chosen to cause either the x or y component of the radar position estimates to converge faster to its true location. This option might be practically valuable because the radar angle relative to an ECAV is more important than its range in terms of minimizing the variance of the phantom track itself. In summary, the linearized system with observer provides great improvement over the unfiltered nonlinear system—at least near the straight ECAV trajectories it was linearized around.

VIII. Conclusion

Position estimation using TDOA techniques was explored and a nonlinear model developed for estimating the position of one radar using two TDOA measurements. Simulating the nonlinear model with a closed-form solution for the position estimate showed that using different ECAV trajectories significantly affects the variance of the estimates.

A linearized time-varying model was developed from the nonlinear one using the ECAV courses as inputs; the model was observable and compared well with the nonlinear model when used to simulate ECAV trajectories. A time-varying Kalman Filter was then constructed and applied to the linearized system. Further analysis of this filtered system showed that the variance of its position estimates for the middle radar converges to zero with time. Simplification of the state covariance matrix showed how choosing certain nominal control inputs, hence ECAV trajectories, can further minimize the variance of the position estimates over a
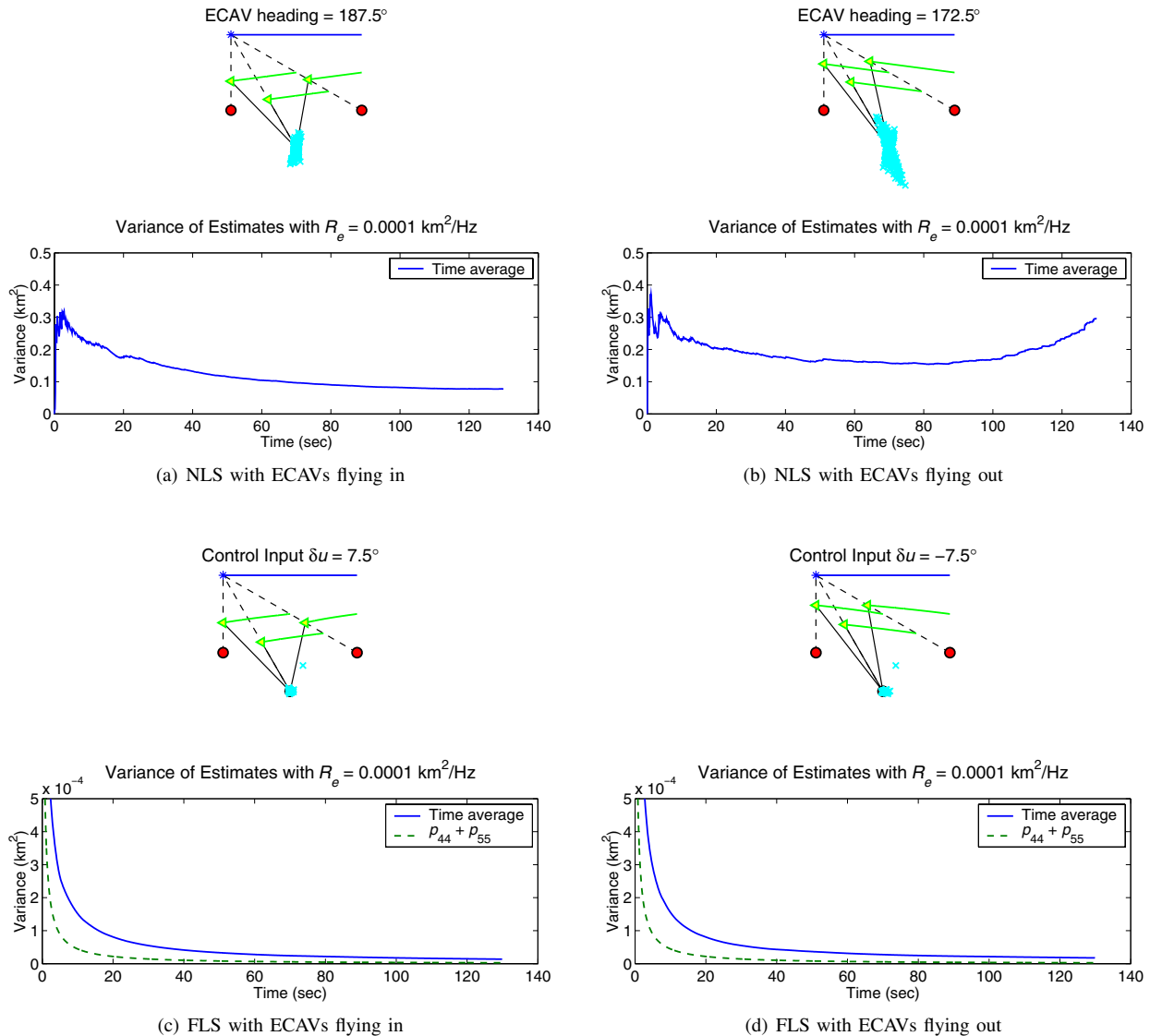
Fig. 6.   Simulations of the Nonlinear System (NLS) for Position Estimation Compared with Simulations of the Filtered Linearized System (FLS)

finite time interval. Comparison of the linearized system with observer to the unfiltered nonlinear system showed through simulation that the linearized system is effective in converging to the true location of the middle radar, whereas the nonlinear system is not. Practically, the performance of the filtered system would depend on how good the initial estimate of the radar location is.

The use of more than two TDOA measurements would increase the estimation accuracy and should be investigated; in this case, with a closed-form solution no longer known, other methods would be required such as nonlinear least squares—see [5]. It would also be beneficial to investigate performance of the Extended Kalman Filter with reasonable initial guesses for the true radar location. Finally, other realistic sources of error in the radar position estimates, such as wind disturbances on the ECAVs and inaccurate ECAV positions, could be included in the system model.

REFERENCES

[1] M. Pachter, P. R. Chandler, R. A. Larson, and K. B. Purvis, "Concepts for generating coherent radar phantom tracks using cooperating vehicles," in *Proc. of the 2004 AIAA Conf. on Guidance, Navigation, and Control*, Providence, RI, Aug. 2004.

[2] K. B. Purvis, P. R. Chandler, and M. Pachter, "Feasible flight paths for cooperative generation of a phantom radar track," in *Proc. of the 2004 AIAA Conf. on Guidance, Navigation, and Control*, Providence, RI, Aug. 2004.

[3] P. Kuykendall and P. V. W. Loomis. In sync with GPS: GPS clocks for the wireless infrastructure. File-8439.pdf. [Online]. Available: http://trl.trimble.com/dscgi/ds.py/Get/File-8439

[4] R. G. Brown and P. Y. C. Hwang, *Introduction to Random Signals and Applied Kalman Filtering*, 3rd ed.   New York: John Wiley & Sons, 1997.

[5] F. Gustafsson and F. Gunnarsson, "Positioning using time-difference of arrival measurements," in *Proc. of the 2003 IEEE International Conf. on Acoustics, Speech, and Signal Processing*, vol. 6, pp. 553–556.

[6] K. J. Åström, *Introduction to Stochastic Control Theory*.   New York: Academic Press, 1970.